Applied Surface Science 360 (2016) 113–120

Contents lists available at ScienceDirect

Applied Surface Science

journal homepage: www.elsevier.com/locate/apsusc

Submicron/nano-structured icephobic surfaces made from fluorinated polymethylsiloxane and octavinyl-POSS

Yancai Li [1], Chenghao Luo [1], Xiaohui Li, Kaiqiang Zhang, Yunhui Zhao, Kongying Zhu, Xiaoyan Yuan *

School of Materials Science and Engineering, and Tianjin Key Laboratory of Composite and Functional Materials, Tianjin University, Weijin Road 92#, Nankai District, Tianjin 300072, China

ARTICLE INFO

Article history:
Received 18 August 2015
Received in revised form 9 October 2015
Accepted 26 October 2015
Available online 31 October 2015

Keywords:
Hybrid films
Fluorinated polymethylsiloxane
OVPOSS
Icephobic properties

ABSTRACT

Fluorinated hybrid films composed of fluorinated polymethylsiloxane (PMHS–*x*FMA, *x* = 6, 13, 17) and octavinyl-polyhedral oligomeric silsesquioxanes (OVPOSS) were prepared for icephobic applications. PMHS–*x*FMA with diverse fluorinated side groups were synthesized *via* hydrosilylation of polymethylhydrosiloxane (PMHS) with fluorinated methacrylate (*x*FMA), *i.e.*, hexafluorobutyl methacrylate (6FMA), tridecafluorooctyl methacrylate (13FMA) and heptadecafluorodecyl methacrylate (17FMA), respectively. Characterizations of atomic force microscope and scanning electron microscope indicated that surfaces of the hybrid films consisted of submicron/nano-scaled OVPOSS aggregates, and the root-mean-square roughness (S_q) could vary from 42.6 nm to 145.2 nm with various OVPOSS content (5–20 wt%). Wettability measurements of the prepared films demonstrated that the relatively longer fluorinated side groups in PMHS–17FMA were beneficial for decreasing surface energy and enhancing hydrophobic properties. However, the fluorinated hybrid films with PMHS–17FMA presented higher ice shear strengths due to the stronger interfacial interactions between the film surface and ice/water. The film prepared by PMHS–13FMA and 10 wt% of OVPOSS with proper roughness (90.2 nm) performed the lowest ice shear strength (188.2 ± 13.4 kPa) among all the samples. Dynamic water droplet impact measurement revealed that the rougher surface with the mass fraction of OVPOSS more than 10 wt% and S_q larger than 90 nm could repel water droplets. The submicron/nano-structured surface of PMHS–*x*FMA and OVPOSS was expected for anti-icing applications.

1. Introduction

Ice accretion on surfaces such as power network systems, aircrafts, buildings, and telecommunication towers may lead to serious safety risks and enormous economic losses [1–3]. To eliminate or decrease the negative impact of icing on surfaces, active and passive strategies have been applied. Since most of the active strategies are inefficient, energy-consuming, high-cost, or environmentally harmful, development of passive anti-icing coatings is urgently desired [4]. In the past few years, a considerable number of measures which can actually reduce icing and ice adhesion strength have been taken [5–10]. From a different perspective, these coatings can be subdivided into 'anti-icing' ones to prevent accretion, and 'icephobic' ones used to remove ice once it has formed [4,7].

In general, surface chemistry and morphology are the principal concerns for conceiving icephobic or anti-icing coatings. The particular properties, such as low surface energy, low glass transition temperature and modulus, endow silicone-based materials remarkable icephobic ability [11,12]. For a commercially available and Pt cured silicone elastomer (Sylgard 184, Dow Corning), Wang et al. revealed an average strength of ice adhesion of 291 ± 44 kPa, which was much lower than 1210 kPa of bare aluminum [13]. Due to the outstanding characteristic of fluorocarbon substitution for obtaining polymer films with low surface energy, it has been found in our previous research that the synergistic effect of silicone and fluorine could reduce the ice shear strength, and the value ~301 ± 10 kPa was significantly lower than that of polyacrylates ~804 ± 37 kPa [14]. Recently, an anti-icing coating with an aqueous lubricating layer was reported by Dou et al., and the ice adhesion strength on these coated surfaces can be lowered to 30.0 kPa [7]. In addition, benefited from the unique structure, fluoro-based

* Corresponding author. Tel.: +86 22 8740 1870; fax: +86 22 8740 1870.
E-mail addresses: yuanxy@tju.edu.cn, xyuan28@yahoo.com (X. Yuan).
[1] Yancai Li and Chenghao Luo contributed equally to this work.

http://dx.doi.org/10.1016/j.apsusc.2015.10.193
0169-4332/

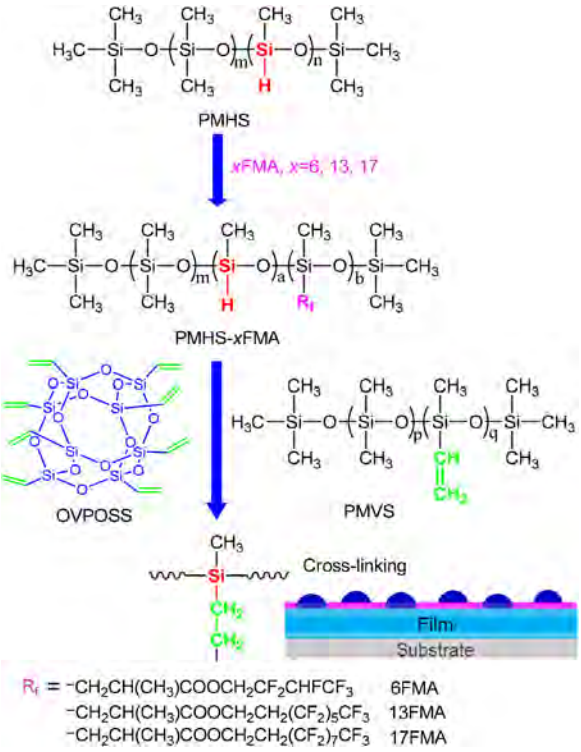

Fig. 1. Synthesis of fluorinated polymethylsiloxane (PMHS–*x*FMA) and formation of hybrid icephobic films from PMHS–*x*FMA and octavinyl-polyhedral oligomeric silsesquioxanes (OVPOSS) based on the addition reaction between vinyl group and Si—H group.

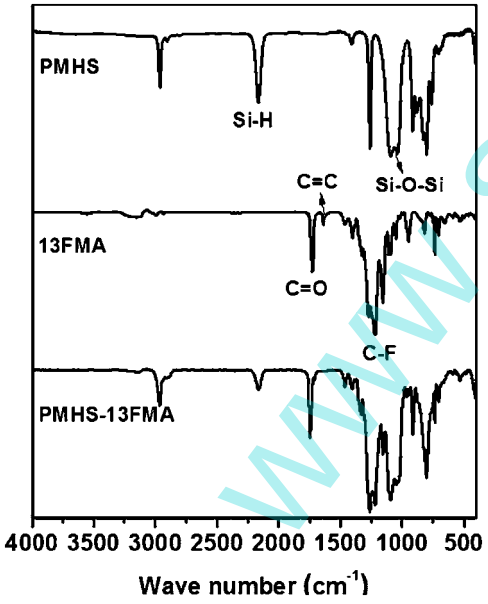

Fig. 2. FT-IR spectra of PMHS, 13FMA and PMHS–13FMA.

polymers also perform excellent water/oil repellency, as well as high chemical resistance [15,16].

The icephobicity of the smooth coatings described above have nearly reached the attainable limit value. It is more likely that further significant reductions in ice adhesion strength can be achieved by incorporating micro-scale and/or nano-scale texture onto surfaces [17–24]. However, the role of surface morphology is complicated. Bharathidasan et al. explored the effect of surface roughness on ice adhesion strength of hydrophilic, hydrophobic

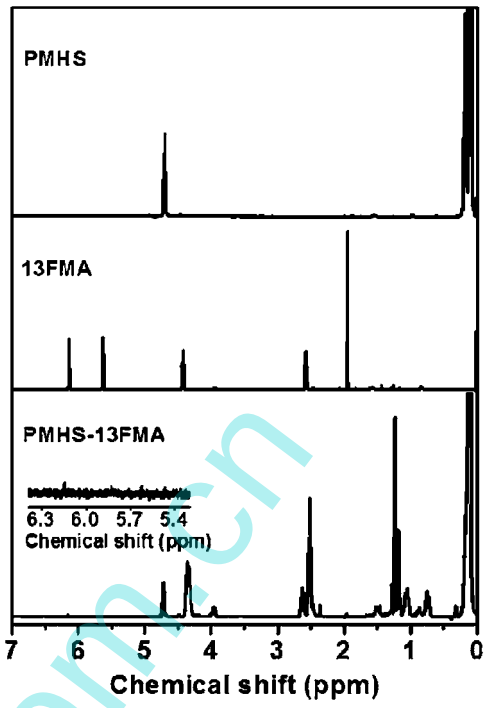

Fig. 3. ^{1}H NMR spectra of PMHS, 13FMA and PMHS–13FMA.

Table 1
Compositions of the fluorinated hybrid films.

Sample	PMHS–*x*FMA[a] (g)	PMVS (g)	OVPOSS (g)	OVPOSS (wt%)
S_{xF-5}	5.0	4.5	0.5	5
S_{xF-10}	5.0	4.0	1.0	10
S_{xF-15}	5.0	3.5	1.5	15
S_{xF-20}	5.0	3.0	2.0	20

[a] PMHS–*x*FMA is referred to PMHS–6FMA, PMHS–13FMA and PMHS–17FMA, respectively.

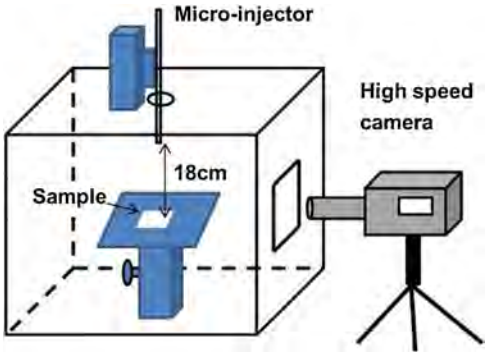

Fig. 4. Schematic depiction of water impact measurement.

Table 2
Surface element composition of the fluorinated hybrid films containing 15 wt% OVPOSS.

Sample	C (atomic %)	O (atomic %)	Si (atomic %)	F (atomic %)	F/Si
S_{6F-15}	46.5	29.2	23.4	0.90	0.04
S_{13F-15}	40.8	20.3	12.4	26.5	2.14
S_{17F-15}	41.8	17.4	11.6	29.2	2.52

and superhydrophobic surfaces, indicating that smooth surface with low surface energy are responsible for low ice adhesion strength [21]. In contrast, Sarkar and Farzaneh described that superhydrophobic surfaces can help mitigate the ice accretion

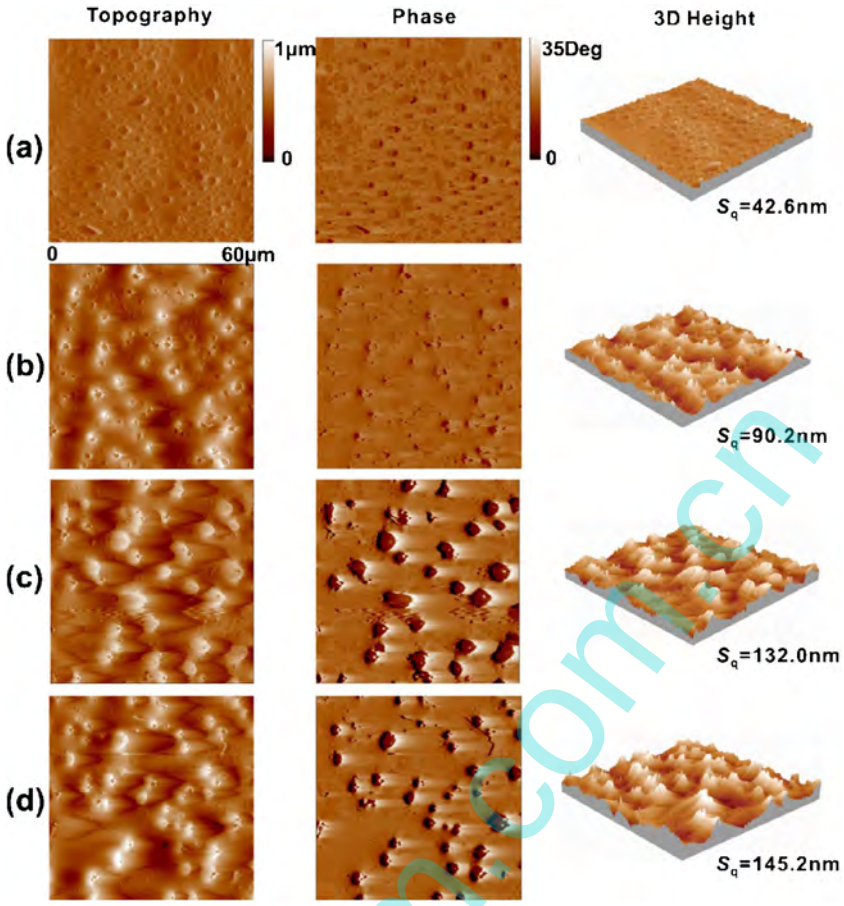

Fig. 5. AFM surface analysis of S_{13F} hybrid films with various mass fractions of OVPOSS. (a) S_{13F-5}, (b) S_{13F-10}, (c) S_{13F-15} and (d) S_{13F-20}.

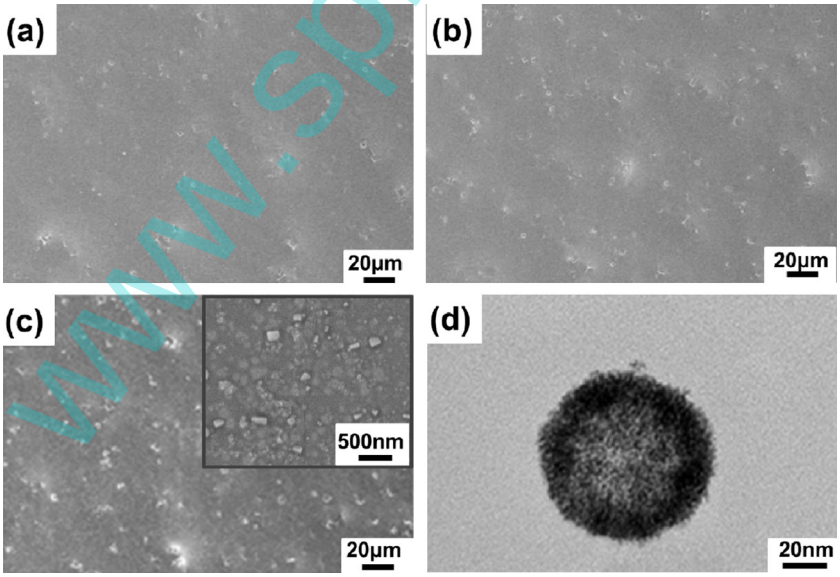

Fig. 6. SEM images of S_{13F-5} (a), S_{13F-10} (b), S_{13F-15} (c) and TEM micrograph of OVPOSS aggregate in α,α,α-trifluorotoluene (d).

problem [22]. Recently, sol–gel icephobic coatings with different roughness were reported, demonstrating that surfaces with roughness ~78 nm displayed the relatively lower ice adhesion strength ~420 kPa, while further increased surface roughness leaded to higher ice adhesion strength, which could be explained by the mechanical interlocking effect between the ice and the surface texture [20,23]. In addition to weaken ice adhesion, the micron/nano-structured morphology also favors the impacted water droplets or condensed micro-droplets detaching from the surface, which is an important capability to avoid ice accretion [24–26].

Although close correlation between surfaces hydrophobicity and ice-repellent behavior has been sought, the corresponding relationship remains controversial. A common theme addressed that

Table 3
Wettability parameters of the fluorinated polymethylsiloxane/OVPOSS hybrid films.

Sample	WCA (°)	θ_{adv} (°)	θ_{rec} (°)	CAH (°)	Surface energy (mJ/m^2)
S_{6F-5}	103.7 ± 0.6	105.3 ± 1.6	97.8 ± 2.3	7.5 ± 0.9	23.3
S_{6F-10}	103.8 ± 0.3	106.3 ± 1.2	98.3 ± 1.3	7.9 ± 2.3	23.3
S_{6F-15}	105.2 ± 0.3	107.2 ± 1.2	99.6 ± 2.2	7.7 ± 3.1	23.3
S_{6F-20}	106.0 ± 1.3	108.4 ± 1.8	91.9 ± 2.5	16.5 ± 3.3	23.4
S_{13F-5}	104.8 ± 2.5	110.3 ± 2.8	98.9 ± 1.2	12.7 ± 2.4	20.3
S_{13F-10}	108.3 ± 0.8	113.7 ± 1.3	96.8 ± 2.9	12.6 ± 2.0	20.5
S_{13F-15}	107.0 ± 0.5	111.2 ± 1.3	99.6 ± 1.4	13.6 ± 1.9	20.3
S_{13F-20}	108.7 ± 1.6	110.9 ± 1.2	94.2 ± 3.2	16.7 ± 2.6	20.4
S_{17F-5}	105.7 ± 0.6	110.1 ± 2.5	91.0 ± 3.7	18.1 ± 2.1	18.9
S_{17F-10}	110.0 ± 1.3	113.6 ± 1.9	94.8 ± 4.9	19.7 ± 3.8	18.4
S_{17F-15}	112.7 ± 1.5	114.2 ± 1.1	94.7 ± 1.5	19.5 ± 0.9	18.5
S_{17F-20}	114.3 ± 1.2	118.6 ± 1.5	88.2 ± 2.2	30.4 ± 3.2	18.0

the ice adhesion strength decreased with increasing water contact angle, whereas others found little relation between the two parameters [27,28]. Several research groups pointed out that the ice adhesion strength may correlate more strongly with contact angle hysteresis (CAH). For superhydrophobic surfaces, Kulinich et al. stressed that the sample with high water contact angle hysteresis was expected for the larger water–solid (and thus ice-solid) area which was negatively for decreasing the ice adhesion strength [18]. Meuler et al. emphasized a strong correlation between the ice adhesion and the practical work of adhesion scaling parameter $[1+\cos\theta_{rec}]$ for liquid water on the non-textured surfaces comprising commercially available polymers and fluorinated polyhedral oligomeric silsesquioxane (fluorodecyl POSS) [28]. However, there is still a lack of understanding ice adhesion strengths in regard of micron- and/or nano-structured surfaces.

We believe the diverse corresponding relationships for ice adhesion and wettability derives from the use of a single parameter to establish some connection. To avoid this problem fundamentally, this paper will focus on the forces acting at the solid–water and solid-ice interface. In the work, three fluorinated polymethylsiloxanes (PMHS–*x*FMA, $x = 6$, 13, 17) with diverse fluorinated side groups were synthesized *via* hydrosilylation of polymethylhydrosiloxane (PMHS) with fluorinated methacrylate (*x*FMA) monomers, *i.e.*, hexafluorobutyl methacrylate (6FMA), tridecafluorooctyl methacrylate (13FMA) and heptadecafluorodecyl methacrylate (17FMA), respectively. Then fluorinated hybrid films composed of PMHS–*x*FMA and octavinyl-polyhedral oligomeric silsesquioxanes (OVPOSS) were prepared by addition-curable process. Here, OVPOSS was not only used to strengthen the cross-linking structure, but also expected to construct submicron/nano-structured surfaces. It will be powerful for the fabrication of icephobic films by modulating the surface energy and morphology. In addition to the interfacial force, the influences of both relative length of fluorinated side groups and surface morphology on hydrophobic and icephobic performances were discussed. The films that combined of anti-icing and icephobic properties would have great potential to deal with the issue of ice accretion.

2. Experimental methods

2.1. Materials

6FMA, 13FMA and 17FMA were supplied by Xuejia Fluorinesilicon Chemical Co., Ltd. (Harbin, China) and used without further purification. Polymethylhydrosiloxane (PMHS, Si—H content 0.75 wt%) and vinyl-polymethylsiloxane (PMVS, vinyl content 0.8 wt%) were obtained from Haiduo and Dayi Chemical Co., Ltd., China, respectively. Octavinyl-polyhedral oligomeric silsesquioxanes (OVPOSS) was purchased from American Hybrid Plastics Co., Ltd. Speier catalyst (tetrahydrofuran solution, 5 mg/mL) was used in hydrosilylation reaction. α,α,α-Trifluorotoluene (TFT) was purchased from Tianjin Heowns Biochem Technologies LLC, Tianjin, China. Aluminum plates with dimensions of 2 cm × 2 cm were used as substrate, and thoroughly rinsed prior to coating. All other reagents used were commercially available.

2.2. Synthesis of PMHS–xFMA and films preparation

PMHS–*x*FMA with different fluorinated side groups were synthesized *via* hydrosilylation reaction, as shown in Fig. 1. A representative procedure of the reaction between PMHS and 13FMA was as follows. 2.0 g PMHS (15 mmol of Si—H), 3.89 g 13FMA (0.6 equivalent mole of Si—H group) and 5.89 g TFT were placed in a 50 mL three-necked round bottom flask under a nitrogen atmosphere with magnetic stirring. Then the reaction was conducted in a water bath for 12 h at 80 °C after the Speier catalyst (100 ppm) was added. The solution was vacuum dried at 40 °C for one day in order to remove the solvent and the remained monomer. The product was confirmed by the appearance of new peaks at 1745 cm^{-1} (C=O) and 1220 cm^{-1} (C—F) in Fourier transform infrared spectra (FT-IR, Fig. 2) as well as 0.7 ppm and 1.0 ppm (Si—CH_2—$CH(CH_3)$—) in proton nuclear magnetic resonance spectra (^{1}H NMR, Fig. 3). The integral intensity of discharge between the new peaks (0.7 ppm and 1.0 ppm) and that of Si—H (4.7 ppm) in ^{1}H NMR was in accordance with the feeding ratio. By comparison, PMHS–6FMA and PMHS–17FMA were obtained under similar conditions as above.

The fluorinated hybrid films were prepared *via* hydrosilylation of PMHS–*x*FMA and OVPOSS (Fig. 1). A given amount of PMVS was added in order to maintain a specific hydride to vinyl ratio. The detailed compositions of fluorinated hybrid films were listed in Table 1. These films were designated as S_{xF-y}, where the subscripts *x*F ($x = 6$, 13, 17) are abbreviations of PMHS–6FMA, PMHS–13FMA and PMHS–17FMA, respectively; and *y* ($y = 5$, 10, 15 and 20 wt%) represented the percentage mass fraction of OVPOSS within the film. Typically process for preparation of S_{13F-5} film, 5 g PMHS–13FMA, 0.5 g OVPOSS, 4.5 g PMVS and Speier catalyst (100 ppm) were dissolved in TFT to obtain a solution at a concentration of 20 wt%. The S_{13F-5} film was prepared by spin-coating of the solution on the treated aluminum plate, which was then heated in an oven at 100 °C for 3 h after complete evaporation of the solvent.

2.3. Characterizations

FT-IR spectra (PerkinElmer, USA) over the range of 4000–400 cm^{-1} and ^{1}H NMR (INOVA 500 MHz and Infinity plus 300WB, USA) were for the structure analysis of the polymers and monomers. Transmission electron microscope (TEM, Tecnai G2 F20 200 kV, the Netherlands) was applied to observe the self-assembly behavior of OVPOSS in the TFT solution. Surface chemistry was characterized by X-ray photoelectron spectroscopy

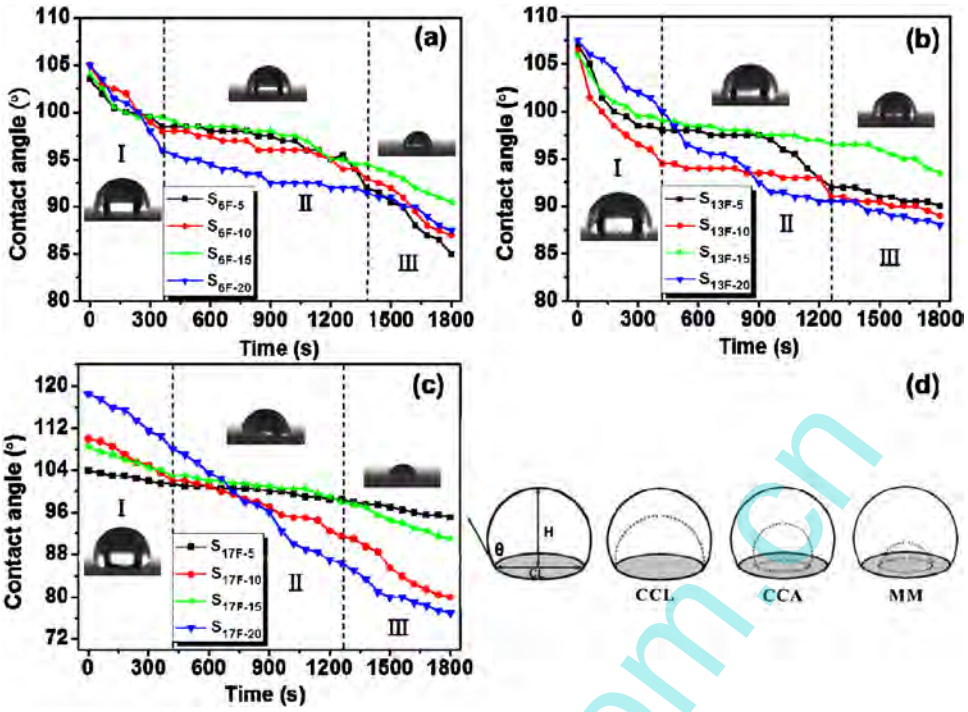

Fig. 7. Evolution of contact angle during the process of droplet evaporation on surfaces (a) S_{6F}, (b) S_{13F}, and (c) S_{17F}. Schematic illustration of different stages is also shown in (d).

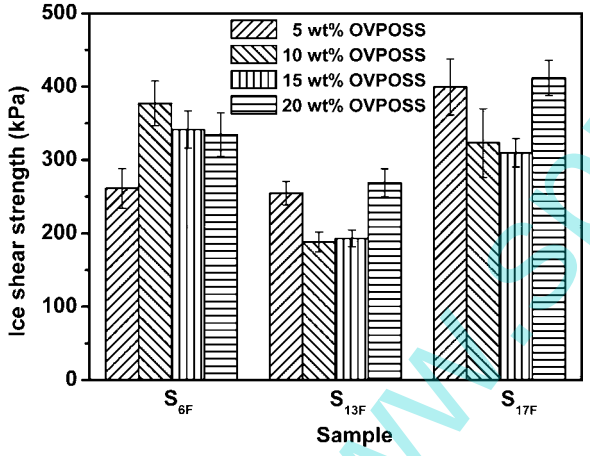

Fig. 8. Ice shear strength of the fluorinated polymethylsiloxane/OVPOSS hybrid films.

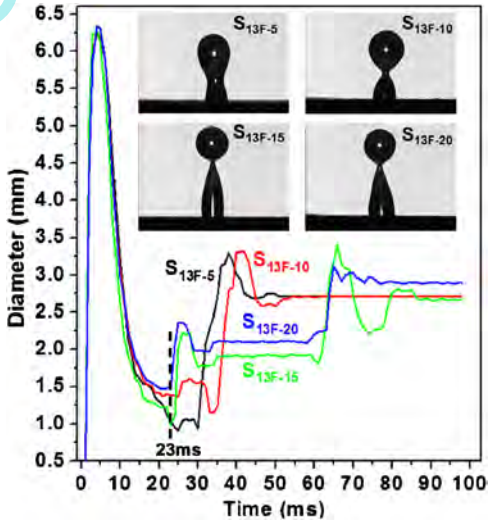

Fig. 9. Evolution of the contact line diameter during the process of droplet impact on horizontal surface of S_{13F} with various mass fraction of OVPOSS. The illustrations were taken from the moment of 23 ms.

(XPS, Perkin-Elmer PHI 5000C ECSA). Both scanning electron microscope (SEM, Hitachi S4800) and atomic force microscope (AFM, CSPM5500A, Being Nano-Instrument, China) operated in tapping mode were applied to analyze surface morphology of the films.

The static contact angle (WCA) was determined by the sessile drop method. 4 μL of the water droplet was gently placed on the testing surface using a micro-syringe and recorded by computer software. Advancing and receding contact angles (θ_{adv} and θ_{rec}) were measured by expanding and withdrawing a drop quasi-statically on horizontal films and their difference was CAH. Deionized water and hexadecane were chosen as the tested liquid, and the Owens-Wendt method was utilized for calculating of surface energy. Each data represented herein was the average of more than five independent measurements.

During water droplet evaporation test, 4 μL deionized water droplet was dispensed on the surface, then the process of consecutive evaporation for 30 min was recorded by a CCD camera at the rate of 1 fps; and the corresponding water contact angle was measured. The whole experiment was conducted at a controlled condition (25 °C, relative humidity was around 60%).

Dynamic drop impact tests were performed on the horizontal or tilted (0° or 30°) film surfaces at room temperature. Water droplet (7 μL) was generated at the tip of a micro-syringe and impacted onto a sample substrate positioned at a controlled distance (18 cm). The motion of the droplet as it impacted the sample was captured with a high speed camera (Olympus i-SPEED LT 4GB Color, Japan) at a frame rate of 1000 fps. The schematic diagram of water impact experiment was shown in Fig. 4.

The method to measure ice adhesion strength has been described in detail previously [14]. Fresh deionized water with a volume of 450 μL was added into the cylindrical glass column; and then the plate cooled to −15 °C at a rate of 2 °C/min and maintained for 3 h to make sure the ice column was fully adhere to the surface. The maximum force (F_{max}) required to detach ice column from its test substrate was measured by the force gauge at a constant velocity of 0.5 mm/s and the ice adhesion strength in shear can be calculated by $\tau = F_{max}/S$, where S is the contact area between ice column and the film. All the samples were tested at least ten times and have been taken their average values.

3. Results and discussion

3.1. Surface composition and morphology

Given that the surface elemental composition has a marked impact on the surface wettability and icephobic properties, the surface compositions of the hybrid films were evaluated by XPS. The contents of carbon, oxygen, fluorine and silicon, as well as the F/Si ratios on the topmost surface of S_{6F-15}, S_{13F-15} and S_{17F-15}, are listed in Table 2. It can be seen that the fluorine content generally increases with elongation of the fluorinated side chains. The fluorine contents on S_{13F-15} (26.5%) and S_{17F-15} (29.2%) surfaces were obviously higher than that on S_{6F-15} (0.9%) surface. The higher fluorine contents on S_{13F-15} and S_{17F-15} surfaces also made higher F/Si ratios. This result indicates that the longer fluorinated side groups in PMHS–13FMA and PMHS–17FMA would migrate easier onto the film surface than the shorter ones in PMHS–6FMA [29].

On the other hand, longer fluorinated side groups in PMHS–13FMA and PMHS–17FMA may shield portion of Si—H groups, which delayed the participation in cross-linking and guaranteed the plenty time for fluorine chains to migrate. In contrast, fluorinated side groups in PMHS–6FMA were apparently shorter, making Si—H groups easily expose and quickly form a network structure during curing period. However, the network structure would limit the migration of fluorinated chains towards surface [30]. That was a key reason for S_{6F-15} presented the lowest fluorine content.

As the surface morphology has a significant influence on the icephobic behaviors [19,20], topographic structures of the hybrid films were further probed using AFM and SEM. Because the effect of OVPOSS on morphologies of the different hybrid films was similar, AFM images of S_{13F} were presented in Fig. 5 as a case study. The bright regions in the topography images represent OVPOSS aggregates that formed on the surface during the spin coating and the solvent evaporation process. When the content of OVPOSS increased to 10 wt%, the surface became rougher and formed a hierarchical structure with submicron/nano-scaled aggregates. Compared with S_{13F-10}, the protrusions on surfaces of S_{13F-15} and S_{13F-20} were more obvious. The root-mean-square roughness (S_q) values of S_{13F-15} and S_{13F-20} were 132.0 and 145.2 nm, respectively, which were larger than those of S_{13F-5} (42.6 nm) and S_{13F-10} (90.2 nm).

As shown in the SEM images of S_{13F} (Fig. 6), OVPOSS aggregates were dispersed well on the surface. The bright submicron/nano-scaled regions were OVPOSS-rich clusters with a uniform distribution (130–220 nm) in the matrix. Consistent with the result of AFM, the surfaces became rougher with increasing the OVPOSS content. According to Ref. [31], OVPOSS could be dispersed in the polymer matrix showing regular cubic crystals in nano-scale dimensions. To magnify the view of the nano-structure, an inset image was added in Fig. 6(c), which indicated that the nano-scale structure could be obtained even when the OVPOSS content was 15 wt%. Additional information about the size of OVPOSS particles can be learned from TEM that is presented in Fig. 6(d). Compared with the size of single OVPOSS molecule [32], OVPOSS in TFT solvent aggregated slightly and displayed regularly spherical with 30–100 nm in size, indicating that surface with submicron/nano-scale roughness could be fabricated with the aid of OVPOSS.

3.2. Wettability

The water contact angles (WCA), contact angle hysteresises (CAH) and surface energies of S_{6F}, S_{13F} and S_{17F} are summarized in Table 3. It can be seen that with the same amount of OVPOSS in films, the WCA of S_{13F} and S_{17F} were higher than those of S_{6F}, and the surface energies of S_{17F} and S_{13F} were lower than those of S_{6F}. This could be attributed to the higher fluorine contents on S_{13F} and S_{17F} surfaces, as confirmed by XPS detection. The WCA of prepared fluorinated hybrid films tended to increase with the increased amount of OVPOSS, ascribed to the rise of surface roughness [20,33]. However, the surface energies were almost the same when the amount of OVPOSS increased, indicating that the loaded OVPOSS had little influence on the surface energy.

Previously, ice adhesion strength was found to be correlated with CAH which was influenced by surface chemistry and roughness [18,34,35]. To some extent, CAH could reflect the interaction force between solid surface and water. Therefore, CAH was tested to analyze the influence of dynamic hydrophobicity on icephobicity. As shown in Table 3, the CAH of S_{17F} (18.1–30.4°) were higher than those of S_{6F} (7.5–16.5°) and S_{13F} (12.6–16.7°), implied surfaces of S_{17F} exerted higher solid–water interaction. Murase et al. pointed out that the adhesion interaction between hydrogen atoms in water and fluorine atom in a fluorocarbon is three times higher than that of the dimethylsiloxane/water system, resulting in increase of CAH on S_{17F} surfaces [36]. Mielczarski et al. have ever investigated thin blend films comprising a cured PDMS matrix and a dispersed surface-active fluorinated/siloxane copolymer [37]. They found that the surface-active copolymer exhibited a remarkable tendency to segregate at the outer surface layer of the blend films, leading to form nanoscale structure on surface. In our work, fluorinated polymethylsiloxane, such as PMHS–17FMA, with longer fluorinated side groups exhibited a more pronounced tendency towards surface segregation than those with shorter fluorinated side groups. The segregation may result in chemical composition heterogeneity which caused the increase of CAH on surfaces of S_{17F} [35].

There were no apparent differences in CAH when OVPOSS content was less than 15 wt% ($S_q \leq 132$ nm) for S_{6F}, S_{13F} and S_{17F}, respectively. But, the hysteresis dramatically increased once mass fraction of OVPOSS beyond this threshold. This may correlate with the increase of solid–water contact area when surface roughness exceeded a critical value.

To reveal more information about the kinetics of interfacial interactions, evolution of contact angle as a result of water droplets evaporation on surfaces of S_{6F}, S_{13F} and S_{17F} were shown in Fig. 7. For S_{6F} and S_{13F}, the variation in contact angle undergoes three stages. First, a nonlinear decrease in the contact angle, but the line of contact remains constant. Second, after the droplet reached a significantly smaller size compared to the initial value, the contact angle remains constant when the contact line decreases. Eventually, the contact angle and contact line were both decreased. The stages, which correspond to the constant contact line mode (CCL), the constant contact angle mode (CCA) and the mixed mode (MM), are illustrated in Fig. 7(d) according to the literature [38]. For samples of S_{17F}, especially for S_{17F-20}, WCA decreased sharply with an almost linear tendency, implying the high interaction between the droplet and solid.

From Fig. 7, it can be drawn that all the films with 15 wt% of OVPOSS displayed the minimum decreased contact angles during

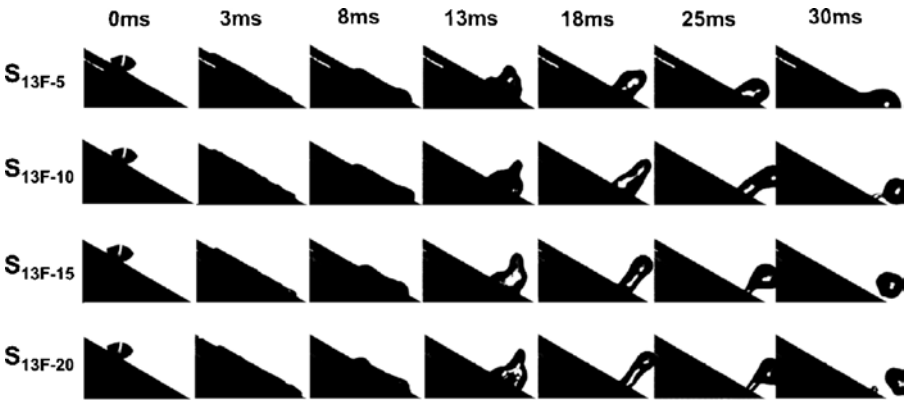

Fig. 10. High speed video images of droplet impact on S_{13F} hybrid films tilted at 30°.

the evaporation processes, while the value of WCA evolvements tended to be the largest when OVPOSS contents increased to 20 wt%. It could be attributed that the surface containing 15 wt% of OVPOSS with roughness of 132.0 nm could support droplet upon the submicron/nano-structures, which promised the minimum contact area between the water droplet and rough surface. However, the excessive roughness would induce the larger solid–water contact area, leading to a marked increase of CAH when OVPOSS contents increased to 20 wt% [18].

3.3. Ice adhesion strength

To predict the icephobic property of the fluorinated polymethylsiloxane/OVPOSS hybrid films, the ice shear strength test was conducted. As shown in Fig. 8, the ice shear strength values of S_{13F} hybrid films were relatively lower than S_{6F} and S_{17F}. Consensus has been reached that the decrease of shear strength of the coated surfaces was due to the reduced surface energy [5,20,33]. Therefore, the higher ice shear strengths on S_{6F} films were mainly associated with their higher surface energy. However, films of S_{17F} owning the lowest surface energy displayed higher ice shear strengths than those of S_{13F}, implying surface energy plays a major but not dominant role on the ice adhesion.

From a perspective of the relationship between wettability and ice adhesion, some studies found correlations between the surface hydrophobicity and the ice adhesion [27,39]. Recently, good correlation between ice adhesion and wetting hysteresis, rather than the water contact angle, was observed [18,40]. For the hybrid films in the article, neither static nor dynamics parameters can be associated with ice adhesion directly. But, the solid–water/ice interaction is expected to become a bridge connecting the wettability and ice adhesion strength.

As analysis of droplets evaporation measurement and CAH data, higher water–solid interaction was proved on surfaces of S_{17F} because of the higher interatomic interaction (hydrogen atoms in water and fluorine atom in fluorocarbon) and chemical composition heterogeneity. According to the literature [4], the binding energies of water molecules to different solids are expected to be similar for water and ice. Thus, the higher ice shear strengths on S_{17F} surfaces could be attributed to the higher interactions between S_{17F} surfaces and water.

When all samples are considered, it is hard to make clear the correlation between surface roughness and ice shear strength. However, for both S_{13F} and S_{17F}, the values of ice shear strength on samples containing 10–15 wt% OVPOSS were always lower than those with the same surface chemistry. The minimum value of ice shear strength decreased to 188.2 ± 13.4 kPa on sample of S_{13F-10}, which was lower than the data of a commercial coating Sylgard 184 (214.9 ± 6.4 kPa, obtained under the same conditions). The establishment of submicron/nano-scaled structures (S_q in range of 90.2–132.0 nm) on hydrophobic surfaces was expected to decrease the solid-ice contact area, and then weakened the ice adhesion strength. Nevertheless, the role of roughness is complicated. The ice shear strength on S_{13F-20} surface was higher than that on S_{13F-15} surface, which could be associated with the larger surface roughness of S_{13F-20}. When the surface roughness was larger than 132.0 nm, the mechanical interlocking effect would happen, resulting in increase of the ice shear strength. This result is in agreement with Ref. [20].

3.4. Droplet impact dynamics

Fluorosilicones is known as "icephobic" material that comprises surfaces with very low surface energy. For these coatings, it can be concluded that the products reduced the amount of energy needed to remove ice but did not prevent ice build-up. In our work, the "anti-icing" ability of the fluorinated polymethylsiloxane/OVPOSS films with submicron/nano-structured surface was further explored.

Fig. 9 shows the evolution of the contact line diameter during droplet impact on horizontal surface of S_{13F}. With a case study of S_{13F-15}, the impacting droplets underwent spreading (0–3.5 ms) and retracting (3.5–23 ms) processes. Curves of S_{13F-5} and S_{13F-10} have similar trend while identical situation appears on S_{13F-15} and S_{13F-20}. Droplets immediately expanded again when the stage of retracting finished on surfaces of S_{13F-5} and S_{13F-10}. In addition, the dynamic behavior of water droplets on surface containing 5–10 wt% OVPOSS appeared to be related to its high sticky ability (see inset in Fig. 9). Samples with 15 wt% and 20 wt% OVPOSS content finished the retraction in the shortest time (around 22 ms) and reached their minimum contact line (1.40 mm and 1.45 mm, respectively), which indicated the minimal resistance of water dynamics.

For ice formation associated with droplet impacted on a surface, the ability to repel water droplets can effectively inhibit build-up of ice on substrates. Fig. 10 displays the dynamic behavior of water droplets dropping on the tilted (30°) S_{13F} surfaces with 18 cm releasing height. It can be seen that water droplets could rebound from film surfaces when OVPOSS content surpassed 10 wt%. As reflected in AFM images, the morphology in Fig. 5(a) are seen to have relatively flatter and shallower tops while the other films are much rougher and sharper. The microstructures would reduce the solid–water contact area when droplets impact on the surfaces, leading to negligible kinetic energy loss. Therefore, the water droplets could bounce off surfaces. Here, for hydrophobic films, we can draw that the rougher of the surface, the stronger of the rebounding ability.

4. Conclusion

A series of fluorinated polymethylsiloxane/OVPOSS hybrid films were prepared *via* hydrosilylation in this study. Wettability and icephobicity of the submicron/nano-structured films with various surface chemistry and morphology have been systematically studied. It suggested that the longer fluorinated side groups in PMHS–13FMA and PMHS–17FMA contributed to strengthen its migration towards the film surface, which was essential for the enhancement of hydrophobicity. However, CAH of S_{17F} (18.1–30.4°) were higher than those of S_{6F} (7.5–16.5°) and S_{13F} (12.6–16.7°) due to the higher solid–water interactions. S_{13F-10} prepared by PMHS–13FMA and 10 wt% of OVPOSS with proper S_q (90 nm) performed the lowest ice shear strength (188.2 ± 13.4 kPa) among all the samples, which was related to the surface energy and surface roughness. The higher ice shear strengths of S_{17F} were attributed to the higher interfacial interactions between film surfaces and ice/water. Dynamic water droplet impact experiment demonstrated that water droplet could bounce off the relatively rougher surface when OVPOSS content is in the range of 15–20 wt%, ascribing to their submicron/nano-structure. Our findings might be useful to understand the relationship between solid–water and solid-ice interaction. More importantly, this investigation opens insights into designing submicron/nano-structured polymer surface materials to have a better performance in practice.

Acknowledgments

This work was financially supported by the National Natural Science Foundation of China (no. 51273146) and Natural Science Foundation of Tianjin, China (no. 14ZCZDGX00008).

References

[1] P. Kim, J. Alvarenga, M.J. Kreder, W.E. Adorno-Martinez, J. Aizenberg, Liquid-infused nanostructured surfaces with extreme anti-ice and anti-frost performance, ACS Nano 6 (2012) 6569–6577.
[2] J. Lv, Y. Song, L. Jiang, J. Wang, Bio-inspired strategies for anti-icing, ACS Nano 8 (2014) 3152–3316.
[3] Q. Liu, Y. Yang, M. Huang, Y.X. Zhou, Y.Y. Liu, X.D. Liang, Durability of a lubricant-infused electrospray silicon rubber surface as an anti-icing coating, Appl. Surf. Sci. 346 (2015) 68–76.
[4] R. Menini, M. Farzaneh, Advanced icephobic coatings, J. Adhes. Sci. Technol. 25 (2011) 971–992.
[5] M. Susoff, K. Siegmann, C. Pfaffenroth, M. Hirayama, Evaluation of icephobic coatings-screening of different coatings and influence of roughness, Appl. Surf. Sci. 282 (2013) 870–879.
[6] L. Zhu, J. Xue, Y. Wang, Q. Chen, J. Ding, Q. Wang, Ice-phobic coatings based on silicon-oil-infused polydimethylsiloxane, ACS Appl. Mater. Interfaces 5 (2013) 4053–4062.
[7] R. Dou, J. Chen, Y. Zhang, X. Wang, D. Cui, Y. Song, L. Jiang, J. Wang, Anti-icing coating with an aqueous lubricating layer, ACS Appl. Mater. Interfaces 6 (2014) 6998–7003.
[8] J. Chen, R. Dou, D. Cui, Q. Zhang, Y. Zhang, F. Xu, X. Zhou, J. Wang, Y. Song, L. Jiang, Robust prototypical anti-icing coatings with a self-lubricating liquid water layer between ice and substrate, ACS Appl. Mater. Interfaces 5 (2013) 4026–4030.
[9] J. Chen, Z. Luo, QF, JL., J. Wang, Anti-ice coating inspired by ice skating, Small 10 (2014) 4693–4699.
[10] M. Ruan, W. Li, B. Wang, B. Deng, F. Ma, Z. Yu, Preparation and anti-icing behavior of superhydrophobic surfaces on aluminum alloy substrates, Langmuir 29 (2013) 8482–8491.
[11] D.M. Yu, Y.H. Zhao, H. Li, H. Qi, B. Li, X.Y. Yuan, Preparation and evaluation of hydrophobic surfaces of polyacrylate-polydimethylsiloxane copolymers for anti-icing, Prog. Org. Coat. 76 (2013) 1435–1444.
[12] M.J. Owen, A review of significant directions in fluorosiloxane coatings, Surf. Coat. Int., B: Coat. Trans. 87 (2004) 71–148.
[13] C. Wang, T. Fuller, W. Zhang, K.J. Wynne, Thickness dependence of ice removal stress for a polydimethylsiloxane nanocomposite: sylgard 184, Langmuir 30 (2014) 12819–12826.
[14] X.H. Li, Y.H. Zhao, H. Li, X.Y. Yuan, Preparation and icephobic properties of polymethyltrifluoropropylsiloxane-polyacrylate block copolymers, Appl. Surf. Sci. 316 (2014) 222–231.
[15] T. Nishino, M. Meguro, K. Nakamae, M. Matsushita, Y. Ueda, The lowest surface free energy based on —CF_3 alignment, Langmuir 15 (1999) 4321–4323.
[16] J.Q. Huang, W.D. Meng, F.L. Qing, Synthesis and repellent properties of vinylidene fluoride-containing polyacrylates, J. Fluorine Chem. 128 (2007) 1469–1477.
[17] T. Aoyama, M. Ishikawa, T. Hirata, Effect of surface roughness on adhesive shear strength between pure ice and a solid surface, Trans. Jpn. Soc. Refrig. Air Cond. Eng. 23 (2011) 273–281.
[18] S.A. Kulinich, M. Farzaneh, How wetting hysteresis influences ice adhesion strength on superhydrophobic surfaces, Langmuir 25 (2009) 8854–8856.
[19] P. Guo, Y. Zheng, M. Wen, C. Song, Y. Lin, L. Jiang, Icephobic/anti-icing properties of micro/nanostructured surfaces, Adv. Mater. 24 (2012) 2642–2648.
[20] Q. Fu, X. Wu, D. Kumar, J.W. Ho, P.D. Kanhere, N. Srikanth, E. Liu, P. Wilson, Z. Chen, Development of sol-gel icephobic coatings: effect of surface roughness and surface energy, ACS Appl. Mater. Interfaces 6 (2014) 20685–20692.
[21] T. Bharathidasan, S.V. Kumar, M.S. Bobji, R.P.S. Chakradhar, B.J. Basu, Effect of wettability and surface roughness on ice-adhesion strength of hydrophilic, hydrophobic and superhydrophobic surfaces, Appl. Surf. Sci. 314 (2014) 241–250.
[22] D.K. Sarkar, M. Farzaneh, Superhydrophobic coatings with reduced ice adhesion, J. Adhes. Sci. Technol. 23 (2009) 1215–1237.
[23] J. Chen, J. Liu, M. He, K. Li, D. Cui, Q. Zhang, Xi. Zeng, Y. Zhang, J. Wang, Y. Song, Superhydrophobic surfaces cannot reduce ice adhesion, Appl. Phys. Lett. 101 (2012) 111603.
[24] L. Mishchenko, B. Hatton, V. Bahadur, J. Ashley Taylor, T. Krupenkin, J. Aizenberg, Design of ice-free nanostructured surfaces based on repulsion of impacting water droplets, ACS Nano 12 (2010) 7699–7707.
[25] M. He, Q. Zhang, X. Zeng, D. Cui, J. Chen, H. Li, J. Wang, Y. Song, Hierarchical porous surface for efficiently controlling microdroplets' self-removal, Adv. Mater. 25 (2013) 2291–2295.
[26] Q. Zhang, M. He, J. Chen, J. Wang, Y. Song, L. Jiang, Anti-icing surfaces based on enhanced self-propelled jumping of condensed water microdroplets, Chem. Commun. 49 (2013) 4516–4518.
[27] A. Dotan, H. Dodiuk, C. Laforte, S. Kenig, The relationship between water wetting and ice adhesion, J. Adhes. Sci. Technol. 23 (2009) 1907–1915.
[28] A.J. Meuler, J.D. Smith, K.K. Varanasi, J.M. Mabry, G.H. McKinley, R.E. Cohen, Relationships between water wettability and ice adhesion, ACS Appl. Mater. Interfaces 2 (2010) 3100–3110.
[29] S. Saidi, F. Guittard, C. Guimon, S. Geribaldi, Fluorinated comblike homopolymers: the effect of spacer lengths on surface properties, J. Polym. Sci., A: Polym. Chem. 43 (2005) 3737–3747.
[30] R. Bongiovanni, G. Malucelli, M. Sangermano, A. Priol, Fluorinated networks through photopolymerisation processes: synthesis, characterization and properties, J. Fluorine Chem. 125 (2004) 345–351.
[31] G. Wen, Z. Qiu, Isothermal crystallization kinetics, morphology, and dynamic mechanical properties of biodegradable poly(ε-caprolactone) and octavinyl-polyhedral oligomeric silsesquioxanes nanocomposites, Ind. Eng. Chem. Res. 51 (2012) 3203–3208.
[32] L. Mate, M. Sjka, A. Strachota, J. Plesloutil, P. Whelan, M. Steinhart, Epoxy networks reinforced with polyhedral oligomeric silsesquioxanes (POSS). Structure and morphology, Macromolecules 37 (2004) 9449–9456.
[33] M. Zou, S. Beckford, R. Wei, C. Ellis, G. Hatton, M.A. Miller, Effects of surface roughness and energy on ice adhesion strength, Appl. Surf. Sci. 257 (2011) 3786–3792.
[34] N.A. Patankar, On the modeling of hydrophobic contact angles on rough surfaces, Langmuir 19 (2003) 1249–1253.
[35] C.W. Extrand, Contact angles and hysteresis on surfaces with chemically heterogeneous islands, Langmuir 19 (2003) 3793–3796.
[36] H. Murase, T. Fujibayashi, Characterization of molecular interfaces in hydrophobic systems, Prog. Org. Coat. 31 (1997) 97–104.
[37] J.A. Mielczarski, E. Mielczarski, G. Galli, A. Morelli, E. Martinelli, E. Chiellini, The surface-segregated nanostructure of fluorinated copolymer-poly(dimethylsiloxane) blend films, Langmuir 26 (2010) 2871–2876.
[38] K.R. Khedir, G.K. Kannarpady, H. Ishihara, J. Woo, S. Trigwell, C. Ryerson, A.S. Biris, Advanced studies of water evaporation kinetics over teflon-coated tungsten nanorod surfaces with variable hydrophobicity and morphology, J. Phys. Chem. C 115 (2011) 13804–13812.
[39] K. Matsumoto, T. Kobayashi, Fundamental study on adhesion of ice to cooling solid surface, Int. J. Refrig. 30 (2007) 851–860.
[40] S.A. Kulinich, M. Farzaneh, Ice adhesion on super-hydrophobic surfaces, Appl. Surf. Sci. 255 (2009) 8153–8157.